ELSEVIER

Contents lists available at ScienceDirect

Organic Electronics

journal homepage: www.elsevier.com/locate/orgel





Coercing assembly of donor-acceptor complexes with hydrogen-bonded frameworks

Anna Yusov¹, Alexandra M. Dillon¹, Chunhua T. Hu, Stephanie S. Lee^{**}, Michael D. Ward¹

Department of Chemistry and Molecular Design Institute, New York University, New York City, New York, 10003, United States

ARTICLE INFO

Keywords:
Hydrogen bonded frameworks
Tetracyanoquinodimethane
Charge transfer
Solid-state organic materials
Single crystal
Crystallography

ABSTRACT

Guanidinium organosulfonate (GS) hydrogen-bonded frameworks (HBFs) constructed from three different naphthalenesulfonates incorporate the electron acceptor tetracyanoquinodimethane (TCNQ) as a guest molecule, with framework architectures that reflect synergy between the persistent 2D hydrogen-bonded GS network and donor-acceptor interactions. The spectroscopic and computational results confirm weak charge-transfer interactions associated with the formation of mixed stacks containing naphthalene donors and TCNQ acceptors that are enforced by the GS framework, suggesting opportunities for the synthesis of new optoelectronic materials through a combination of molecular and crystal design.

1. Introduction

The importance of Professor Martin Pope to organic electronics cannot be overstated. The embodiment of a humble, yet brilliant, scientist, Professor Pope laid the foundation for the field in the early 1960s while a faculty member at New York University in lower Manhattan, with the discovery of electroluminescence in anthracene single crystals [1,2], to be followed by groundbreaking findings of charge-transfer excitons in anthracene, tetracene and perylene crystals [3,4]. There is little doubt that these seminal discoveries are responsible for technologies taken for granted today, from solar panels to organic light emitting diode displays. Years later, in 1982, Professor Pope, with co-author Charles E. Swenson, cemented his position as a founding authority with his 1300-page book "Electronic Processes in Organic Crystals and Polymers," [5] which likely can be found in any laboratory consumed with organic electronics. The authors dedicate this article, which is modest by comparison, to the memory of Professor Pope.

Charge transfer (CT) complexes can be broadly defined as the association of an electron-rich moiety (donor) and an electron-poor moiety (acceptor) wherein electronic charge is transferred from the donor (D) to acceptor (A). In 1973, shortly after the discoveries by Martin Pope, a benchmark example of this class of materials was reported, a 1:1 cocrystal of the donor tetrathiafulvalene (TTF) and acceptor tetracyano-quinodimethane (TCNQ) that exhibited metallic behavior [6–10]. Over

the following five decades, CT complexes have been evaluated for applications from electronics to nonlinear optics [11–22], with an eye towards modulating electronic properties through manipulation of molecular and solid-state structure. Crystalline CT complexes can be described according to segregated stacking motifs (separate ..D..D..D.. and ..A..A..A. stacks), like TTF-TCNQ [23], or mixed stacks (alternating ..D..A..D..A..), like TTF-TCNQF2 [24]. The arrangement of donors and acceptors in the solid state influences their emergent properties, prompting strategies for controlling their assembly using intermolecular interactions, such as π - π stacking, hydrogen bonds and halogen bonds [25–28], application of external pressure during the crystallization process [29], and tuning stoichiometry [30].

Hydrogen-bonded frameworks (HBFs) are a versatile class of materials constructed from organic building blocks that can form crystalline inclusion compounds containing guest molecules [31]. The library of guanidinium organosulfonate (GS) HBFs, first reported by our laboratory in 1994 [32], rely on charge-assisted N–H···O hydrogen bonds formed between guanidinium cations and sulfonate anions to generate a robust 2D quasi-hexagonal hydrogen bonded sheet (Fig. 1). The wide range of organosulfonates, combined with framework isomerism, have permitted the design and synthesis of inclusion compounds for molecular structure determination [33], separation of regioisomers [34], directed aggregation of dyes [35], non-linear optics [36], pheromone encapsulation [37], and controlled orientation of thiophenes [38],

^{*} Corresponding author.

^{**} Corresponding author.

E-mail addresses: stephlee@nyu.edu (S.S. Lee), mdw3@nyu.edu (M.D. Ward).

 $^{^{1}}$ Equivalent first-author contribution.

among other examples [31,39,40]. Donor-acceptor complex formation between the organic residues of GS frameworks and guest molecules has, however, been limited to a single example, a guanidinium azobenzene disulfonate host framework with TTF guests [38].

The modularity of the GS frameworks permits inclusion of a wide range of guest molecules by various GS hosts that can adopt an assortment of framework architectures. This characteristic offers opportunities to enforce the formation of donor-acceptor complexes and manipulate their associated charge-transfer interactions in a way that is not possible with co-crystals alone, whether the organic substituent appended to the sulfonate group is a donor and the guest an acceptor, or viceversa. Herein, we describe GS inclusion compounds based on a

family of naphthalenesulfonates and TCNQ guests. This work demonstrates the utility of GS frameworks to coerce the formation of CT complexes between a weak donor and strong acceptor that otherwise is not stable on its own, while also revealing the influence of donor-acceptor interactions on framework structures. These observations suggest that GS frameworks are promising candidates for the synthesis of CT complexes with emergent properties resulting from directed organization in the solid state.

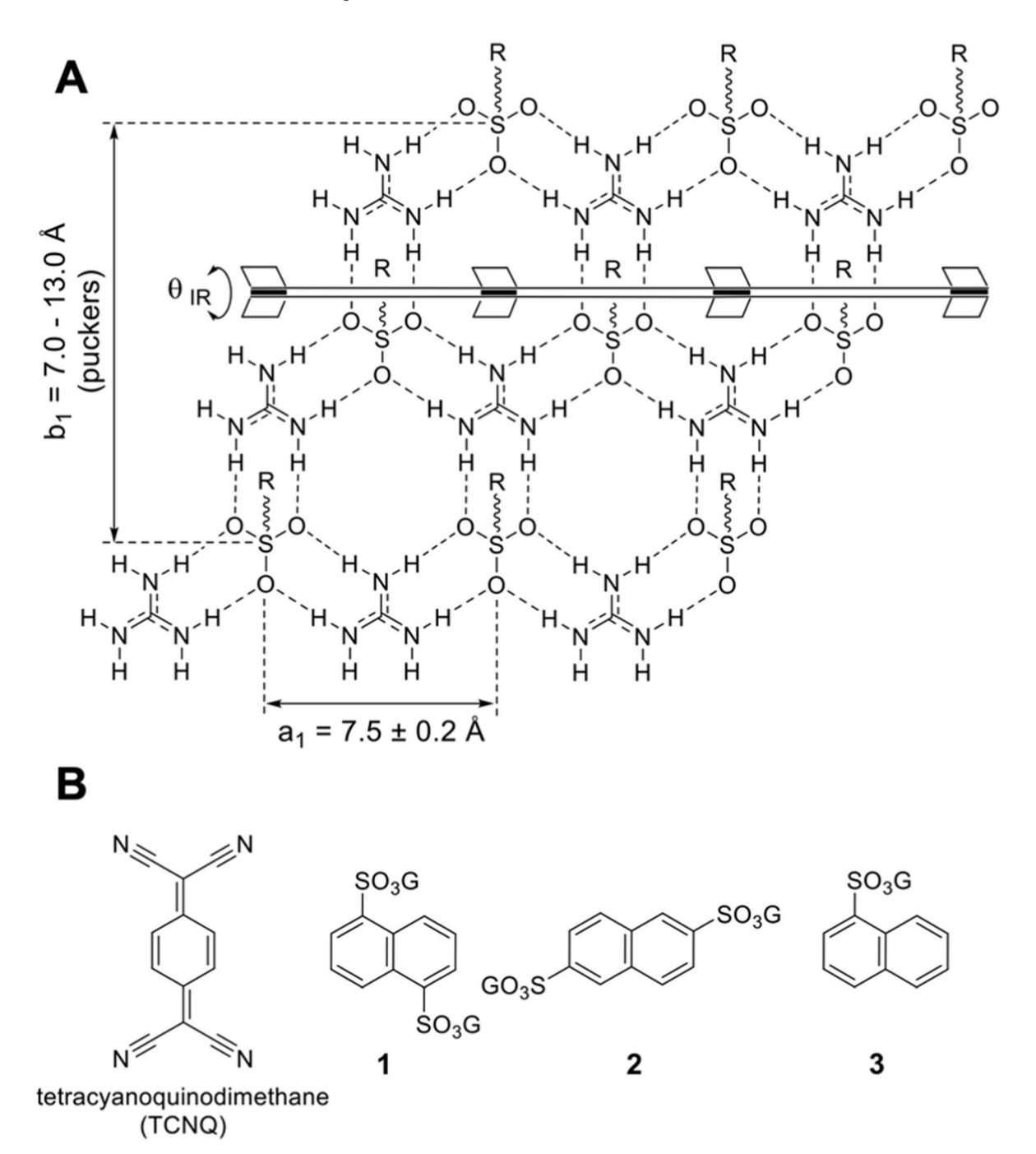


Fig. 1. (A) The quasihexagonal hydrogen-bonded guanidinium organosulfonate (GS) 2D sheet, which can be described as hydrogen-bonded ribbons fused along their edges. The sheet can pucker with a puckering angle, θ_{IR} , about a flexible "hinge" connecting the ribbons, allowing for accommodation of guest molecules. R groups can project on either side of the sheet and are responsible for growth of the framework along the third dimension. (B) Molecular structure of TCNQ and the three GS hosts examined in this study.

2. Experimental section

2.1. Materials and methods

2.1.1. Materials

7,7,8,8-tetracyanoquinodimethane (TCNQ) was purchased from Tokyo Chemical Industry Co., Ltd (Tokyo, Japan). The various organosulfonic acids or their sodium salts were purchased from Sigma Aldrich. Solvents were purchased from Fisher Scientific.

2.1.2. Preparation of guanidinium napthalenesulfonates

Sodium salts of the sulfonic acids were converted to the acid form by elution through an Amberlyst 36 ion-exchange column. Guanidinium organosulfonates salts were prepared by combining acetone solutions containing approximately 1.10 molar equivalents of guanidinium tetrafluoroborate and 1.0 molar equivalents of a selected organosulfonic acid, which produced a precipitate of the corresponding GS salt, sometimes referred to as an "apohost." Alternatively, approximately 1.0 molar equivalents of the organosulfonic acid host and approximately 1.10 molar equivalents of guanidinium tetrafluoroborate were combined in water, the mixture dried in vacuo, and the resulting solid filtered and washed with acetone several times, affording the GS salt apohost in nearly quantitative yield.

2.1.3. Crystallization of donor-acceptor inclusion compounds

Acetonitrile:methanol solutions (1:1) containing equimolar (0.01 M) amounts of the respective GS salt apohost and TCNQ were allowed to evaporate slowly under ambient conditions. These crystallizations produced red-orange crystals with needle-like habit for compounds ${\bf 1}$ and ${\bf 2}$ and plate-like habit for compound ${\bf 3}$ after several days.

2.2. Characterization

2.2.1. Single crystal X-ray diffraction

Single crystal X-ray diffraction data for inclusion compounds 1-3 were obtained using a Bruker SMART APEX II diffractometer equipped with a PHOTON-II-C14 detector. The X-ray beam generated from an INCOTEC micro-focused Mo source was monochromated and collimated by a Montel multilayer optics. The wavelength from the Mo $\mbox{\rm K}\alpha$ radiation is 0.71073 Å. Crystal temperature was controlled by an Oxford Cryosystems 700+ Cooler. Crystals were mounted on a MiTeGen Micro-Mount with Type B immersion oil (Cargille Labs). A phi scan (APEX4) was performed for each crystal to evaluate crystal quality and determine the data collection parameters. Full datasets were collected with omega scan methods [41]. The data sets were processed with the INTEGRATE program of the APEX4 software for reduction and cell refinement. Multi-scan absorption corrections were applied by the SCALE program for the area detector. Structures were solved by intrinsic phasing methods (SHELXT) and the structure models were completed and refined using the full-matrix least-square methods on F^2 (SHELXL) [42, 43]. Non-hydrogen atoms in the structures were refined with anisotropic displacement parameters, and hydrogen atoms on carbons were placed in idealized positions (C–H = 0.95-1.00 Å) and included as riding with $U_{\rm iso(H)} = 1.2$ or 1.5 $U_{\rm eq(non-H)}$. Disordered solvent in compound 1 that could not be modeled properly based on the electron density distributions and its contributions were treated by PLATON/SQUEEZE routine (Spek) [44]. Crystallographic data of these structures, including cif, res, fcf, and hkl files, have been deposited with the Cambridge Crystallographic Data Centre (CCDC) with Numbers 2206745-2206747. Copies of these data can be requested, free of charge, from the CCDC website at https://www.ccdc.cam.ac.uk/structures/.

2.2.2. Spectroscopic Measurements

Raman spectra were recorded on a Raman microscope (DXR, Thermo Fisher Scientific, Waltham, MA) using a 785 nm excitation laser operating at 20 mW, with a $2~{\rm cm}^{-1}$ accuracy and slit width of 50 mm. The

data were analyzed using the Omnic software package. IR absorption spectra were recorded on an IR microscope (Nicolet iN10 MX, Thermo Fisher Scientific, Waltham, MA) with a 4 cm⁻¹ resolution. The data were analyzed using the Omnic software package. Solution absorption data were collected at room temperature using solutions containing equimolar amounts of TCNQ and guanidinium naphthalenesulfonate apohost salt in a 1:1 methanol/acetonitrile mix, using a MDFlexStation 3 plate reader. Emission data was collected with a 390 nm excitation using a MDFlexStation 3 plate reader. Solid-state optical absorption and emission spectra for crystals 1–3 were measured using a CRAIC Technologies 508 PV microscope spectrophotometer in the range of 400–1000 nm, equipped with halogen and mercury lamps and a linear array CCD detector. Aperture size and objective were consistent across all crystals. Emission data were collected using a fluorescence cube for excitation at 436 nm.

2.3. Calculations

Hirshfeld surface calculations were executed for the single crystal data of the naphthalene-TCNQ co-crystal and each inclusion compound using the CrystalExplorer software [45], equipped with Tonto computational backend. Time dependent-density functional theory (TD-DFT) calculations were performed using the Gaussian 16 package [46]. The electronic excitation spectra were simulated at the B3LYP/6-311G(d,p) level for the first 20 excited states of each donor-acceptor pair, where each crystal structure was modified by replacing $-SO_3$ groups with an aromatic proton. Molecular orbitals were visualized using MO visualizer in GaussView 6.0.16 [47] with an isovalue of 0.02 and a course cube grid.

3. Results and discussion

3.1. Crystal structures

GS inclusion compounds based on guanidinium 1,5-naphthalene disulfonate (G)₂(1,5-NDS), guanidinium 2,6-naphthalene disulfonate (G)₂(2,6-NDS) and guanidinium 1-naphthalene monosulfonate (G)(1-NMS) were crystallized by slow evaporation of methanol-acetonitrile solutions prepared by dissolving their respective GS apohost salts and an equimolar amount of TCNQ. This protocol produced single crystals of $(G)_2(1,5-NDS)\supset TCNQ$ (1), $(G)_2(2,6-NDS)\supset (TCNQ)_2$ (2) and $(G)(1-CNQ)_2$ NMS)⊃TCNQ (3) (Fig. 2, Table S1, Figs. S1-4). The quasi-hexagonal GS motif was consistent throughout, but the framework architecture differed among the compounds, affording uniquely organized TCNQ guests and some surprising structural features. All three inclusion compounds were stable under ambient conditions, reflecting stability conferred by the tethering of the naphthalene donor to the hydrogen bonded sheet. In contrast, naphthalene-TCNQ co-crystals were reported to be unstable under ambient conditions [48], which is likely due to weak CT character and the volatility of naphthalene.

 $(G)_2(1,5\text{-NDS})\supset TCNQ$ (1) crystallized as a red-orange needle in the rhombohedral space group $R\overline{3}$, in which six GS ribbons fused along their edges curl into a cylinder and sulfonate groups on opposite sides of the naphthalene residue bridge adjacent cylinders (Fig. 3). The inside of the cylinder contained disordered solvent, which was removed by PLATON/SQUEEZE. Although the cylindrical architecture has been observed before, it has been limited to trisulfonates with three-fold symmetry [49] and monosulfonates [50]. In the case of 1, the cylindrical architecture was unexpected in the absence of a threefold-symmetric topological generator. Previous reports with the $(G)_2(1,5\text{-NDS})$ host have demonstrated that the lamellar architecture can accommodate guest molecules that are sufficiently small to fit in the narrow channels formed by this "stubby" pillar [51]. For example, this lamellar architecture is observed in $(G)_2(1,5\text{-NDS})$ adiponitrile (CSD Refcode: TUQNIC) [51]. While the diameter of the linear adiponitrile guest can be accommodated by the

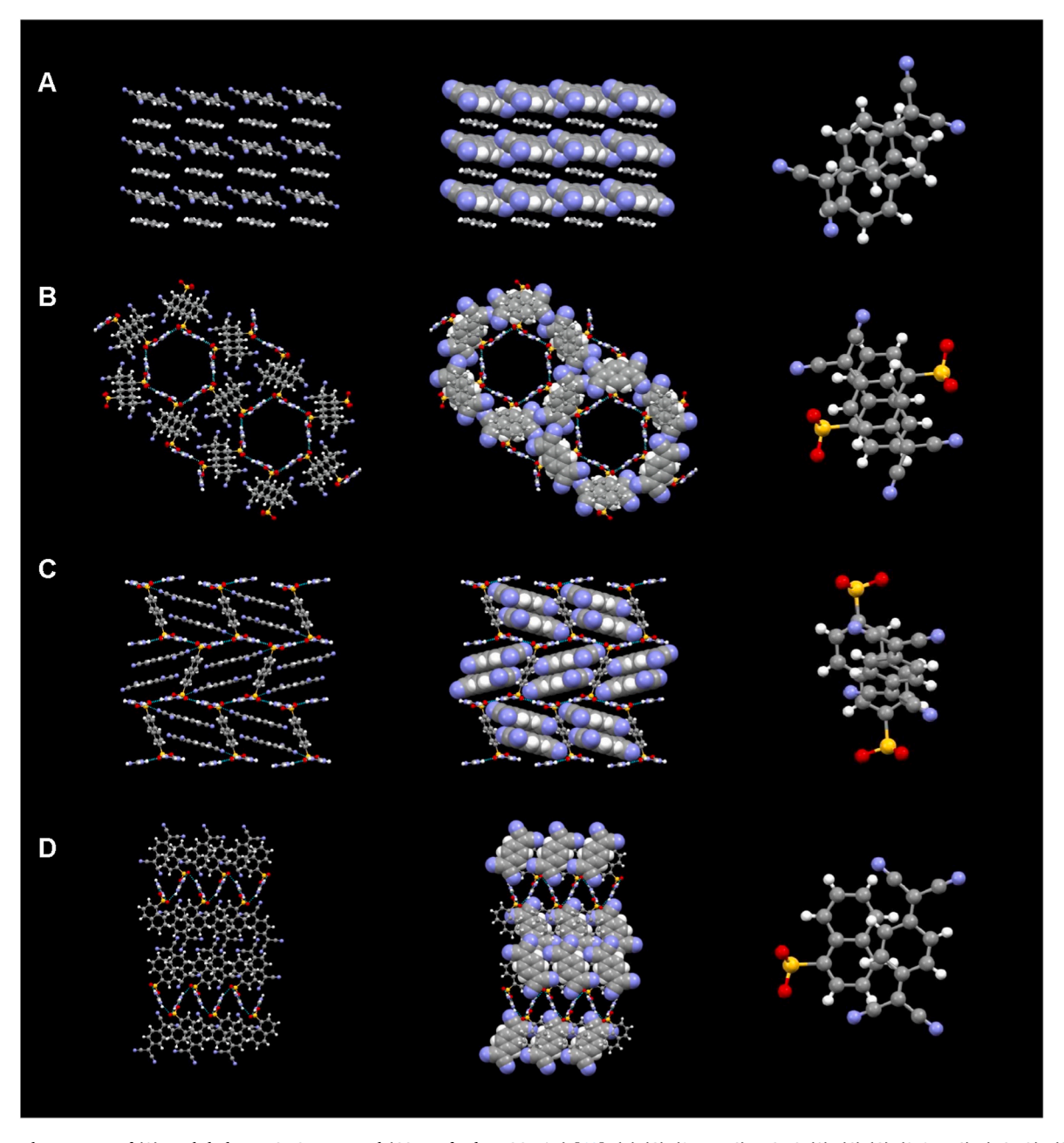


Fig. 2. Crystal structures of (A) naphthalene-TCNQ co-crystal (CSD Refcode: TCQNAP) [48], (B) $(G)_2(1,5\text{-NDS})$ \supset TCNQ (1), (C) $(G)_2(2,6\text{-NDS})$ \supset (TCNQ) $_2(2)$, (D) (G) (1-NMS) \supset TCNQ (3). The structures in the left and center columns are rendered as ball and stick (left) and with TCNQ guest molecules as space filling (center). The rightmost column depicts the overlap of the naphthalene and TCNQ constituents (right).

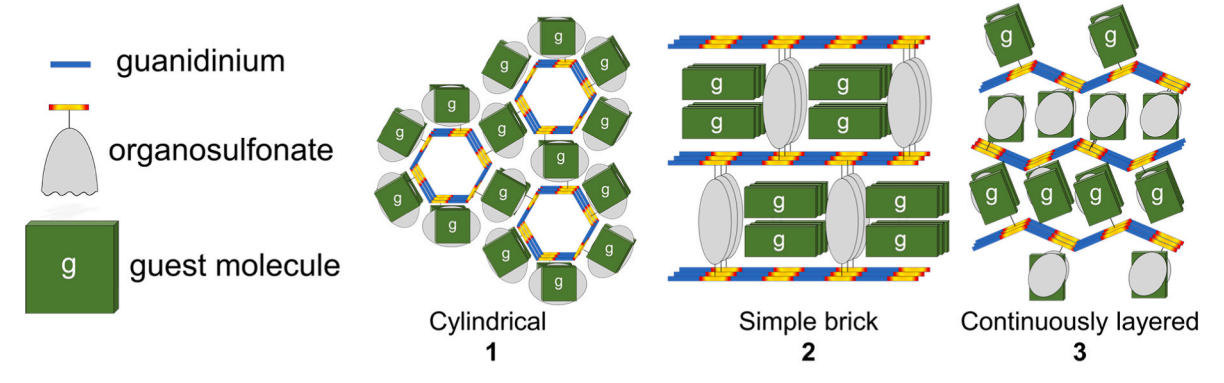


Fig. 3. Schematic representation of the GS framework architectures for compounds 1–3.

channels in the lamellar architecture of the $(G)_2(1,5\text{-NDS})$ host, the span across both the long and short axes of TCNQ precludes a face-to-face orientation of a TCNQ guest, whether its long axis would be parallel or perpendicular to the GS sheet. Consequently, the host reconciles the steric challenge by adopting the observed unique cylindrical architecture wherein TCNQ guests reside between the naphthalene residues in a mixed-stack donor-acceptor motif.

The crystal structure and stoichiometry of (G)₂(2,6-NDS)⊃(TCNO)₂ (2) is distinct from the rhombohedral compound, crystallizing as a redorange needle in the space group $P2_1/n$. The GS framework adopts the simple brick architecture in which naphthalene pillars bridge parallel GS sheets, forming channels that accommodate face-to-face TCNQ dimers organized edge-to-edge along the channel (Fig. 3). Unlike the 1,5-NDS pillar in compound 1, the longer 2,6-NDS pillar allows for the inclusion of larger guest molecules in the more common lamellar architecture. In this case, the angle between the planes of naphthalene and TCNQ guest molecules is 59° (Fig. 2C, left). Close contacts between the nitrogen atom of the TCNQ guests and the guanidinium proton suggest that hydrogen bonding between the guest and the GS framework may play some role in the formation of the inclusion compound, with the distance between the two atoms shorter than that of the sum of the van der Waals radii of the two atoms (3.060 Å). The centroid-to-centroid distances between TCNQ dimer molecules in compound 2 are shorter than the corresponding distances in the crystal structure of TCNQ alone (4.499 Å vs 5.683 Å, respectively; CSD Refcode: TCYQME) [52], likely reflecting a "lattice pressure" exerted by the hydrogen-bond reinforced channels that coerces the TCNQ molecules in each dimer into a less slipped conformation (Fig. S5). The ability of GS frameworks to influence the aggregation of guest molecules has been previously demonstrated for laser dyes [35], polyconjugated molecules [38] and luminescing guests [53–55].

(G)(1-NMS)⊃TCNQ (3) crystallizes as a red-orange plate in the space group Pnma, adopting the so-called continuously layered inclusion compound (CLIC) architecture (Fig. 3) [50]. This architecture is observed often for guanidinium monosulfonate inclusion compounds [50], wherein the organic residues of the sulfonate interdigitate to create cavities that accommodate guest molecules. In the case of 3, however, the larger guest molecule forces adjacent layers to associate through their narrow edges, likely supported by cyano-cyano dipole-dipole interactions between opposing TCNQ guests and weak (naphthalene)C-H···N=C(TCNQ) hydrogen-bonds. The distance between opposing GS sheets is larger as compared to typical examples with the CLIC architecture, which accommodates the long axis of the TCNO guest [50]. Notably, the hydrogen bonded sheet is highly puckered (ca. 75°), which can be attributed to the reduced degree of interdigitation of opposing layers. The naphthalene residues and TCNQ guests stack in an alternating manner along the crystallographic b-axis, resulting in a mixed-stack donor-acceptor motif.

Donor-acceptor properties are influenced by many structural factors stacking motif, interplanar separation, offset of donor and acceptor – that affect orbital mixing, HOMO-LUMO separations and associated charge-transfer absorption energies [56]. Compounds 1 and 3 exhibit mixed stacks of naphthalene donors and TCNQ acceptors, similar to the aforementioned naphthalene-TCNQ co-crystal (CSD Refcode: TCQNAP) [48]. The fast growth axes in both compounds 1 and 3 are along the direction of the charge transfer stacks (c and b axes, respectively). The interplanar angles between naphthalene and TCNQ in the naphthalene-TCNQ co-crystal, 1, and 3 are 13.23°, 8.22°, and 0°, respectively, suggesting that the GS sheet enforces a more parallel arrangement of donor and acceptor molecules (Table S2). Measuring interplanar distances between non-parallel planes is inexact, however, requiring other approaches for comparing donor-acceptor overlap. Notably, the centroid-to-centroid donor-acceptor distance is slightly shorter in 1 than in the naphthalene-TCNO co-crystal (3.542 Å vs 3.937 Å, respectively; Table S2), reflecting a reduced offset of the donor and acceptor rings in 1 and suggestive of more substantial donor-acceptor

interaction (Fig. 2, right). The centroid-to-centroid donor-acceptor distance is, however, larger for 3 (4.520 Å) because of a significant offset of each donor-acceptor (Figs. 2 and 4; Table S2). The lattice parameters along the stacking directions in 1 and 3, which are defined by the intraribbon sulfur-sulfur distances ($d_{S...S}$), are less than that in the naphthalene-TCNQ co-crystal, suggesting an important role for hydrogen-bonding in the enforcement of mixed stacks. Moreover, the $d_{S...S}$ values in 1 and 3 (7.085 Å and 6.850 Å, respectively) are shorter than those typically observed along the GS ribbons in either the lamellar or cylindrical architectures ($a_1 = 7.5 \pm 0.2 \text{ Å}$, Fig. 1A), suggesting donor-acceptor interactions surprisingly compress the guanidinium sulfonate ribbons along the mixed-stack direction. Despite the smaller $d_{S...S}$ value in 3, the smaller centroid-to-centroid distance in 1 would be expected to result in more substantial donor-acceptor interaction. It is reasonable to expect that the different donor-acceptor motifs observed among these compounds would be manifested in different charge transfer properties.

Previous reports of donor-TCNQ charge-transfer complexes have used Hirshfeld surfaces [57-59] to assess the interactions between the TCNO cyano nitrogen and the donor protons as a metric of donor-acceptor intermolecular interaction [60]. Hirshfeld surfaces are calculated by dividing a crystal into regions in which the electron distribution of a sum of spherical atoms for the molecule (the promolecule) dominates the sum over the crystal (the procrystal) [59]. These surfaces can then be portrayed as 2D "fingerprint plots" of d_i (distance from a point on the surface to the nearest nucleus inside the surface) versus d_e (distance from a point on the surface to the nearest nucleus outside the surface). Hirshfeld surfaces are unique for every crystal structure and are sensitive to minor changes in inter- and intramolecular interactions, providing a more global insight into these interactions than a single atom to atom measurement. A longer "antennae" on the 2D fingerprint plots is associated with mutually short d_i and d_e distances, signifying a stronger interaction. The structural features of compounds 1-3 were characterized further through the calculation of their Hirshfeld surfaces, and the fingerprint plots reveal two strong and sharp "antennae" indicative of the strong charge-assisted hydrogen bond interactions between the guanidinium protons and the sulfonate oxygens. These antennae are absent in the naphthalene-TCNQ co-crystal (Fig. 5A). The (TCNQ)C≡N···H–C(naphthalene) interactions are highlighted in Fig. 5B for the naphthalene-TCNQ co-crystal and compounds 1-3. The longer antennae in the highlighted regions for compounds 1-3 reveal that the (TCNO)C≡N···H-C(naphthalene) interactions are stronger than in the naphthalene-TCNQ co-crystal. Although Hirshfeld surfaces do not inform on the degree of charge transfer in these compounds, they can provide insight into the crystal packing that influences their emergent properties.

3.2. Emergent properties

The Raman spectra of compounds **1–3** were collected to evaluate the extent of charge transfer between the naphthalene donors and TCNQ acceptors [61–64]. A modest shift to lower frequencies in the C=C stretching signal was observed in compounds **1–3**, ($\nu_{CC}=1440~{\rm cm}^{-1}$, 1442 cm⁻¹ and 1447 cm⁻¹, respectively) as compared to crystalline TCNQ ($\nu_{CC}=1448~{\rm cm}^{-1}$). The largest shift is observed in **1**, consistent with a larger degree of charge transfer in this compound, and a negligible amount in compounds **2** and **3** (the C=C stretch for a TCNQ⁻ anion is observed at 1395 cm⁻¹ ⁶¹) (Fig. 6, Fig. S6). No significant shift in the C=N stretch was observed in the Raman spectra. Previous reports, however, have suggested that using the C=N stretch in Raman spectra as a diagnostic for the degree of charge-transfer is unreliable [64,65], suggesting IR spectroscopy could provide complementary insights.

A similar trend was identified in solid-state IR measurements, wherein inclusion compounds 1–3 demonstrated a shift in the C \equiv N stretching signal to lower wavenumbers as compared to a TCNQ only sample (the TCNQ⁰ and TCNQ⁻ anion ν_{CN} stretch is observed at 2225

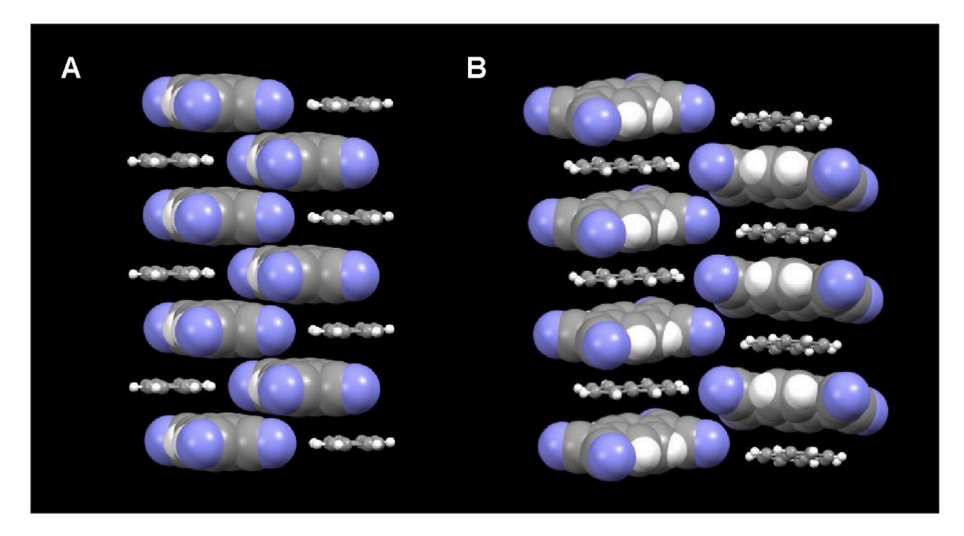


Fig. 4. Donor-acceptor packing in mixed stacked compounds (A) 1 and (B) 3 with naphthalene host represented as ball-and-stick and TCNQ as spacefilling. Sulfonate and guanidinium moieties are hidden for clarity.

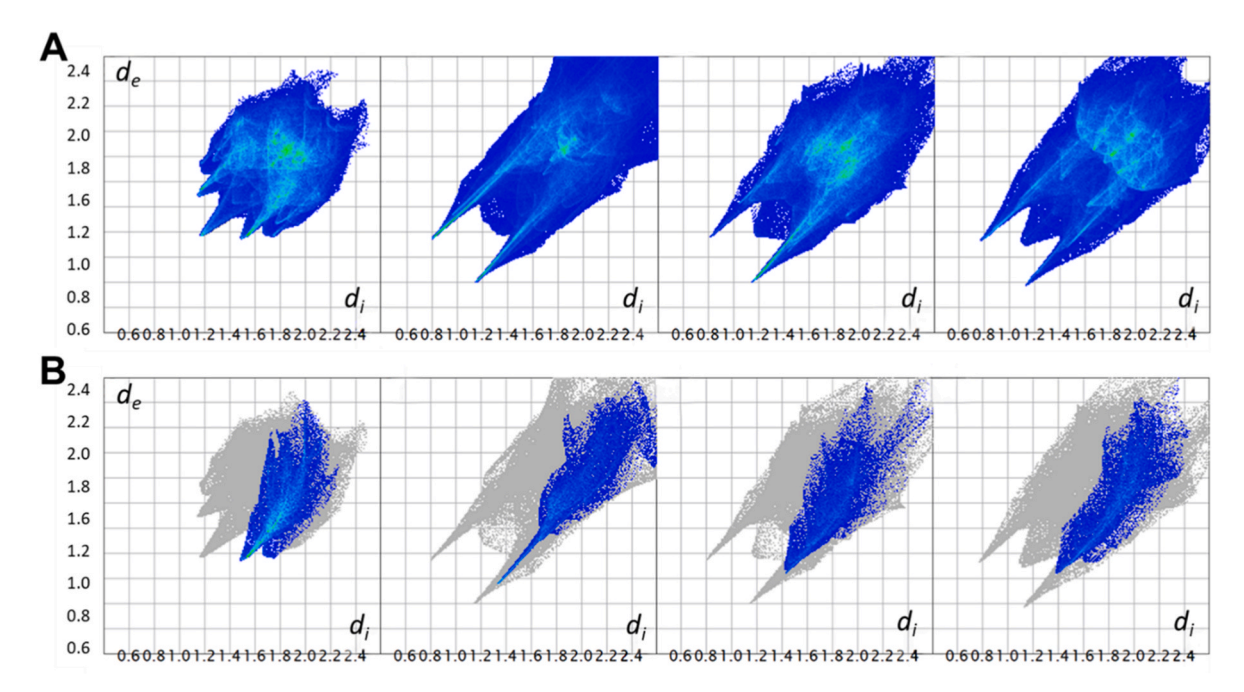


Fig. 5. Fingerprint plots derived from the Hirshfeld surfaces of the naphthalene-TCNQ co-crystal and inclusion compounds 1–3 (left to right). (A) Full surface. (B) Surface with (TCNQ)C—N···H—C(naphthalene) close contacts unveiled.

 ${\rm cm}^{-1}$ and 2181 ${\rm cm}^{-1}$, respectively) [66] (Fig. 6, Fig. S7). Two well-defined peaks are observed for 1 ($v_{CN} = 2225 \text{ cm}^{-1}$ and 2214 ${\rm cm}^{-1}$), consistent with two different pairs of C \equiv N bond lengths (1.138 and 1.151 Å). Broadening of the v_{CN} peaks was observed for 2 and 3 (v_{CN} = 2224 cm⁻¹ and 2221 cm⁻¹, respectively), which can be attributed to the four unique distances in these structures (1.142, 1.143, 1.146, 1.150 Å and 1.139, 1.147, 1.160, 1.174 Å, respectively). The shift in these C≡N stretches may also be impacted by short (TCNQ)C≡N···H-C (naphthalene) nearest neighbor distances observed for compounds 1-3 (2.433, 2.622 and 2.643 Å, respectively). The degree of charge transfer (ρ) can be estimated from the observed shift of the ν_{CN} stretch to lower wavenumbers using eq. (1), which has been employed to calculate ρ for a family of TCNQ charge-transfer compounds [66]. The degree of charge transfer based on $\nu_{CN}=2227$ - 44ρ eq. (1) decreases in the order 1 ($\rho=$ $(0.30) > 3 (\rho = 0.14) > 2 (\rho = 0.07)$ (Fig. S8) where the degree of charge transfer in 2 is negligible, which is expected for the nearly orthogonal

arrangement of TCNQ with respect to the donor.

The absorption spectra of naphthalene and TCNQ and the components of compounds $1{\text -}3$ in solution, measured with a 1:1 stoichiometry, exhibited maxima at 390 nm that can be attributed to TCNQ alone, with no significant differences among these combinations above 270 nm (Fig. S9). Using a 390 nm excitation wavelength, these solutions each exhibited minimal fluorescence maxima near 620 nm that can be attributed to TCNQ alone (Fig. S10). These spectra provide evidence of the absence of donor-acceptor complexes in solution under these conditions.

Single crystals of inclusion compounds 1–3 exhibited absorbance with maxima of 550 nm, 430 nm, and 520 nm, respectively (Fig. 7). In compounds 1 and 3 the shapes of the excitation curves indicated a sharp transition, suggesting that calculation of Tauc plots could be used to estimate the charge-transfer transition energy associated with the donor-acceptor complexes (Fig. S11) [67]. This analysis suggested that

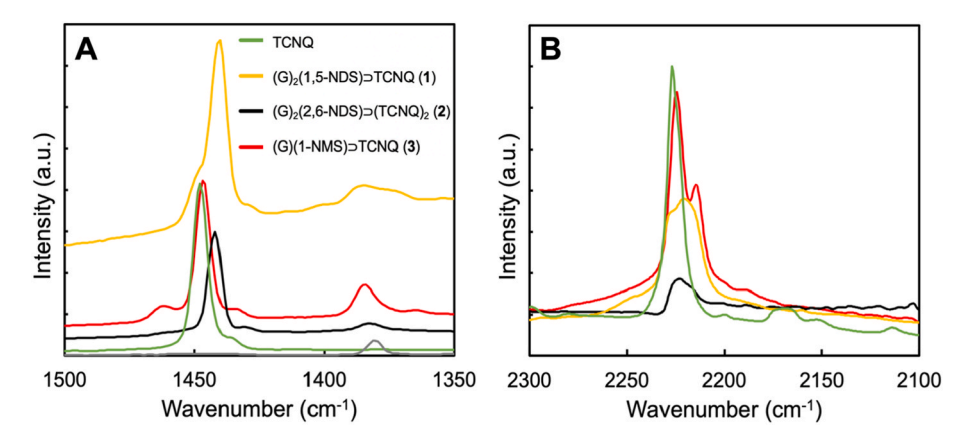


Fig. 6. (A) Raman spectra of TCNQ and compounds 1–3 in the region of the v_{CC} stretching mode. (B) Infrared spectra of TCNQ and compounds 1–3 in the region of the v_{CN} stretching mode. The legend applies to both panels (A) and (B).

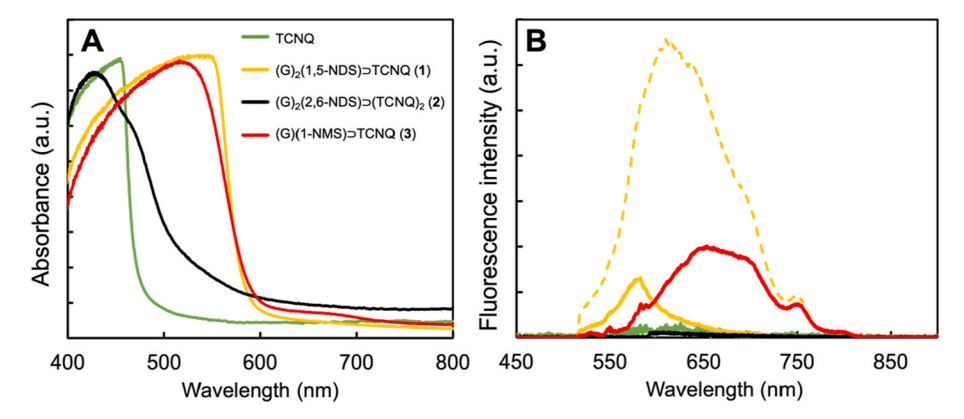


Fig. 7. (A) Absorption spectra of TCNQ and inclusion compounds 1–3 and (B) emission spectra of TCNQ and inclusion compounds 1–3 excited at 436 nm. The dashed line for compound 1 corresponds to the emission from the (001) face of the crystal, and the solid line for compound 1 corresponds to the emission from the (110) face of the crystal. Compound 2 is plotted and exhibits negligible intensity. The legend applies to both panels (A) and (B).

the energy gap associated with the CT transition was similar in compounds 1 and 3, and relatively higher in 2, which further supports the observation of less favorable CT stacking in inclusion compound 2. Using an excitation wavelength of 436 nm, strong fluorescence was observed for compounds 1 (at 617 and 590 nm) and 3 (at 660 nm) (Fig. 7). Compound 1 crystallizes with a needle-like habit with its long axis oriented along the [001] direction, with the sides of the needle bounded by (110) and $(1\overline{1}0)$ faces. The dashed and solid lines for compound 1 correspond to emission from the (001) and (100) faces of the crystal, respectively (Fig. 7B). The differences in the fluorescence observed for these two faces can be attributed to the crystallographic anisotropy of the crystal. Notably, fluorescence was negligible for compound 2, in which TCNQ guests are isolated dimers oriented nearly perpendicular to the plane of the 2,6-NDS pillar such that donor-acceptor interaction is not anticipated. Consequently, the observation of fluorescence appears to be a signature of donor-acceptor interactions, supported by the presence of fluorescence for 1 and 3 and its absence for 2.

The contributing frontier molecular orbitals for compounds $1{\text -}3$ were calculated and visualized to assess the charge transfer and local transitions, where hybridization of molecular orbitals of the donor and acceptor molecules is required for charge transfer (Fig. 8) [68]. Time-dependent density functional theory (TD-DFT) (B3LYP/6-311G(d, p) level of theory, gas-phase) was used to calculate the molecular orbitals involved in the electronic excitation spectra for each inclusion compound structure, based on their respective crystal structures without guanidinium ions and sulfonate residues (sulfonate groups were replaced with an aromatic proton) (Figs. S12–S14). The various

contributing frontier molecular orbitals from the calculated UV-vis spectra for the excited state with the greatest oscillator strength were analyzed (Tables S3-S5). The transitions contributing to the excited state with the greatest oscillator strength for inclusion compounds 1-3 are HOMO(-2)→LUMO and HOMO(-1)→LUMO for 1, HOMO(-2)→ LUMO for 2, and HOMO(-3)→LUMO and HOMO(-2)→LUMO for 3 (Table S6). The calculated UV-vis spectra for the naphthalene/TCNQ pairs in 1 and 3 do not exactly match the experimental solid-state UV-vis data for compounds 1 and 3 (Table S7), which exhibit a broad absorption signal that may be attributable to a dispersion of states derived from frontier orbitals that are extended along the mixed stacks in the crystal, rather than the single donor-acceptor pair used in the calculations. The greatest HOMO-LUMO splitting is observed for the naphthalene/TCNQ pairs in compound 1, followed by 3, with negligible changes in energy of the HOMO and LUMO in compound 2, as compared to HOMO of naphthalene and the LUMO of TCNQ alone. In the case of the naphthalene/TCNQ pair in compound 2, the electronic transition stems solely from the orbitals resembling the HOMO and LUMO of TCNQ, with no donor-acceptor state mixing. For the naphthalene/TCNQ pairs in 1 and 3, however, the electron density from the contributing molecular orbitals for the excited state with the greatest oscillator strength exists on both the naphthalene donor and TCNQ acceptor for compounds 1 and 3, consistent with the presence of charge-transfer (Fig. 8). The greatest orbital mixing and HOMO-LUMO splitting is observed for 1, further supporting a larger degree of orbital mixing and associated charge transfer compared with 3.

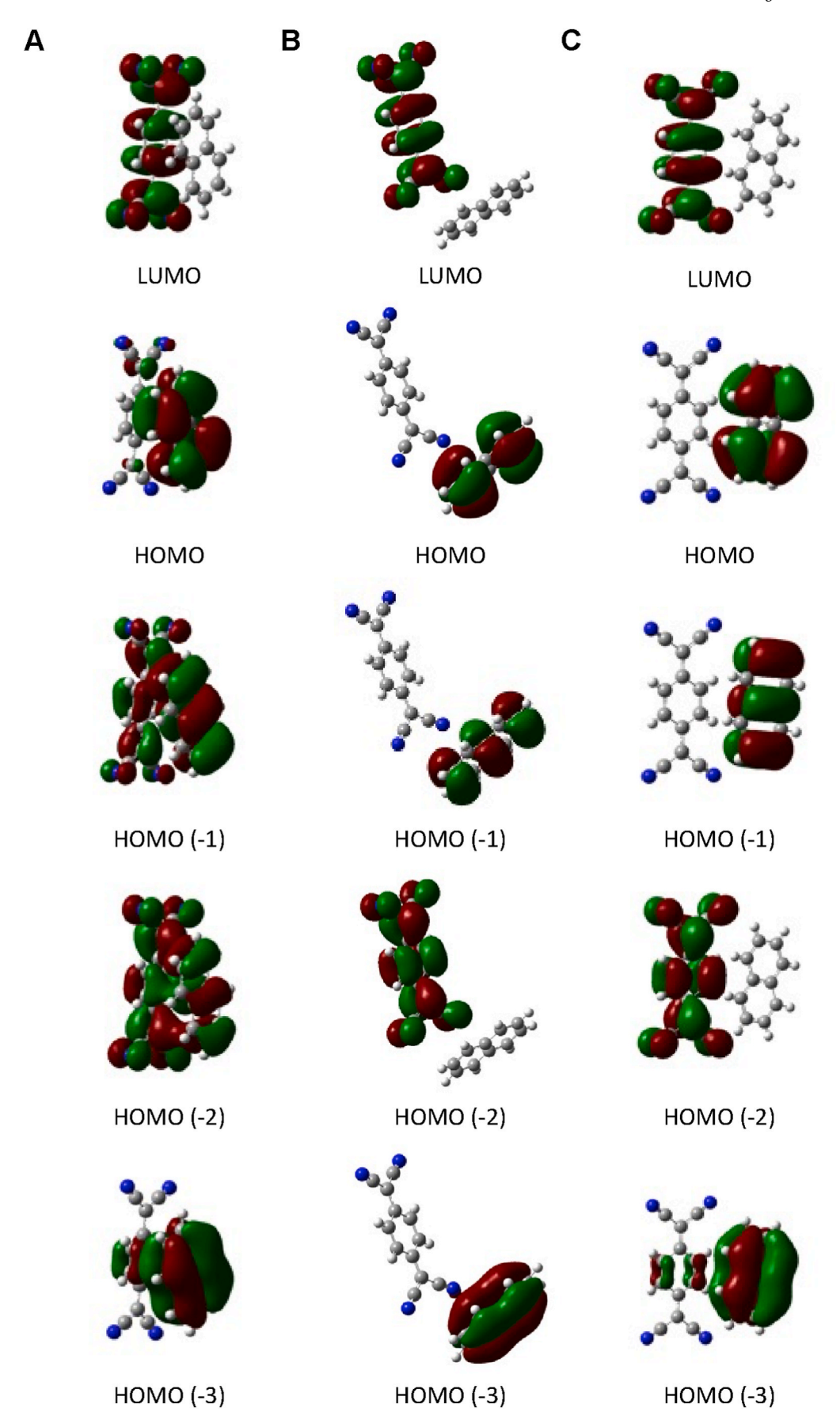


Fig. 8. The contributing frontier molecular orbitals for naphthalene/TCNQ pairs in (A) 1, (B) 2, and (C) 3 calculated by TD-DFT. Important transitions for each compound: (A) HOMO(-2) \rightarrow LUMO and HOMO(-1) \rightarrow LUMO, (B) HOMO(-2) \rightarrow LUMO, (C) HOMO(-3) \rightarrow LUMO and HOMO(-2) \rightarrow LUMO.

4. Conclusion

Three inclusion compounds comprising donor naphthalene hosts and acceptor TCNQ guests exhibit three distinct architectures, some unexpected. Analysis of the single crystal structures revealed a synergistic role of structural enforcement by hydrogen bonding in the GS sheet and donor-acceptor interactions in guiding inclusion compound formation and subsequent donor-acceptor motifs. Vibrational spectroscopy revealed the degree of charge transfer, albeit slight as expected for the weakly donating naphthalene moiety. Yet the compound with the greatest degree of charge transfer - compound 1 - exhibited the strongest emission, consistent with the assignment to frontier orbital mixing along the mixed stacks. Finally, TD-DFT revealed the greatest amount of orbital mixing in compound 1 between donor and acceptor, consistent with some degree of charge-transfer. Collectively, these findings suggest GS frameworks can be used to modulate donor-acceptor organization and the strength of charge-transfer interaction, paving the way toward controlled design of new and tunable functional materials.

Declaration of competing interest

The authors declare that they have no known competing financial interests or personal relationships that could have appeared to influence the work reported in this paper.

Data availability

Data will be made available on request.

Acknowledgments

This work was supported by the National Science Foundation Grant Opportunities for Academic Liaison with Industry (GOALI) program through award no. DMR-2002964 and the NSF Chemistry Research Instrumentation and Facilities Program (CHE-0840277). Additionally, AY was supported by the Margaret Strauss Kramer Fellowship. This work was also supported in part through the NYU IT High Performance Computing resources, services, and staff expertise. The authors would like to thank Dr. Henry Towbin for his assistance with solid state IR measurements, conducted at Columbia University's Lamont-Doherty Earth Observatory.

Abbreviations

1-NMS 1-naphthalene monosulfonate
1,5-NDS 1,5-naphthalene disulfonate
2,6-NDS 2,6-naphthalene disulfonate

A acceptor D donor

CCD charge-coupled device

CCDC Cambridge Crystallographic Data Centre CLIC continuously layered inclusion compound

CT charge transfer

CSD Cambridge Structural Database

G guanidinium

GS guanidinium organosulfonate HBFs hydrogen bonded frameworks

IR infrared

HOMO highest occupied molecular orbital LUMO lowest unoccupied molecular orbital

MO molecular orbital

TCNQ tetracyanoquinodimethane

TD-DFT time dependent density functional theory

TTF tetrathiafulvalene

Appendix A. Supplementary data

Supplementary data to this article can be found online at https://doi.org/10.1016/j.orgel.2023.106752.

References

- M. Pope, H.P. Kallmann, P. Magnante, Electroluminescence in organic crystals, J. Chem. Phys. 38 (8) (1963) 2042–2043, https://doi.org/10.1063/1.1733929.
- M. Sano, M. Pope, H. Kallmann, Electroluminescence and band gap in anthracene,
 J. Chem. Phys. 43 (8) (1965) 2920–2921, https://doi.org/10.1063/1.1697243.
- [3] M. Pope, H. Kallmann, J. Giachino, Double-quantum external photoelectric effect in organic crystals, J. Chem. Phys. 42 (7) (1965) 2540–2543, https://doi.org/ 10.1063/1.1666320
- [4] N. Geacintov, M. Pope, H. Kallmann, Photogeneration of charge carriers in tetracene, J. Chem. Phys. 45 (7) (1966) 2639–2649, https://doi.org/10.1063/ 11727084
- [5] Pope, M.; Swenson, C. E. Electronic Processes in Organic Crystals and Polymers; Oxford University Press: New York, Oxford.
- [6] J. Ferraris, D.O. Cowan, V. Walatka, J.H. Perlstein, Electron transfer in a new highly conducting donor-acceptor complex, J. Am. Chem. Soc. 95 (3) (1973) 948–949, https://doi.org/10.1021/ja00784a066.
- [7] L. Wu, F. Wu, Q. Sun, J. Shi, A. Xie, X. Zhu, W. Dong, A TTF-TCNQ complex: an organic charge-transfer system with extraordinary electromagnetic response behavior, J. Mater. Chem. C 9 (9) (2021) 3316–3323, https://doi.org/10.1039/ DOTG-5230B
- [8] Y. Takahashi, K. Hayakawa, T. Naito, T. Inabe, What happens at the interface between TTF and TCNQ crystals (TTF = tetrathiafulvalene and TCNQ = 7,7,8,8tetracyanoquinodimethane)? J. Phys. Chem. C 116 (1) (2012) 700–703, https://doi.org/10.1021/jp2074368.
- [9] J.R. Kirtley, J. Mannhart, When TTF met TCNQ, Nat. Mater. 7 (7) (2008) 520–521, https://doi.org/10.1038/nmat2211.
- [10] S.A. Odom, M.M. Caruso, A.D. Finke, A.M. Prokup, J.A. Ritchey, J.H. Leonard, S. R. White, N.R. Sottos, J.S. Moore, Restoration of conductivity with TTF-TCNQ charge-transfer salts, Adv. Funct. Mater. 20 (11) (2010) 1721–1727, https://doi.org/10.1002/adfm.201000159.
- [11] K. Bechgaard, K. Carneiro, M. Olsen, F.B. Rasmussen, C.S. Jacobsen, Zero-pressure organic superconductor: di- (Tetramethyltetraselenafulvalenium)-Perchlorate [(TMTSF)2ClO4], Phys. Rev. Lett. 46 (13) (1981) 852–855, https://doi.org/ 10.1103/PhysRevLett.46.852.
- [12] J.S. Miller, Extended Linear Chain Compounds, first ed., Plenum Press, New York, 1982 vols. 1-3.
- [13] J. Zhang, W. Xu, P. Sheng, G. Zhao, D. Zhu, Organic donor–acceptor complexes as novel organic semiconductors, Acc. Chem. Res. 50 (7) (2017) 1654–1662, https://doi.org/10.1021/acs.accounts.7b00124.
- [14] M.D. Ward, Linear chain organometallic donor-acceptor complexes and one-dimensional alloys. Synthesis and structure of [(.Eta.6-C6Me3H3)2M][C6(CN)6] (M = iron, ruthenium), Organometallics 6 (4) (1987) 754–762, https://doi.org/10.1021/cm00147a013.
- [15] J.M. Williams, J.R. Ferraro, R.J. Thorn, K.D. Carlson, U. Geiser, H.H. Wang, A. M. Kini, M.-H. Whangbo, Organic Superconductors (Including Fullerenes). Synthesis Structure, Properties, and Theory, first ed., Prentice-Hall, Inc., Englewood Cliffs, New Jersey, 1992.
- [16] D. Braga, F. Grepioni, in: D. Braga, F. Grepioni, A.G. Orpen (Eds.), Crystal Engineering: from Molecules and Crystals to Materials BT - Crystal Engineering: from Molecules and Crystals to Materials, Springer Netherlands, Dordrecht, 1999, pp. 421–441, https://doi.org/10.1007/978-94-011-4505-3_24.
- [17] D. Braga, L. Maini, L. Prodi, A. Caneschi, R. Sessoli, F. Grepioni, Anions derived from squaric acid form interionic π-stack and layered, hydrogen-bonded superstructures with organometallic sandwich cations: the magnetic behaviour of crystalline [(H6-C6H6)2Cr]+[HC4O4], Chem. Eur J. 6 (8) (2000) 1310–1317, https://doi.org/10.1002/(SICI)1521-3765(20000417)6:8<1310::AID-CHEM1310>3.0.CO, 2-T.
- [18] X. Liang, Q. Zhang, Recent progress on intramolecular charge-transfer compounds as photoelectric active materials, Sci. China Mater. 60 (11) (2017) 1093–1101, https://doi.org/10.1007/s40843-016-5170-2.
- [19] C. Dai, Z. Wei, Z. Chen, X. Liu, J. Fan, J. Zhao, C. Zhang, Z. Pang, S. Han, Efficient two-photon excited fluorescence from charge-transfer cocrystals based on centrosymmetric molecules, Adv. Opt. Mater. 7 (22) (2019), 1900838, https://doi. org/10.1002/adom.201900838.
- [20] V.W.-W. Yam, A.K.-W. Chan, E.Y.-H. Hong, Charge-transfer Processes in metal complexes enable luminescence and memory functions, Nat. Rev. Chem 4 (10) (2020) 528–541, https://doi.org/10.1038/s41570-020-0199-7.
- [21] W. Wang, L. Luo, P. Sheng, J. Zhang, Q. Zhang, Multifunctional features of organic charge-transfer complexes: advances and perspectives, Chem. Eur J. 27 (2) (2021) 464–490, https://doi.org/10.1002/chem.202002640.
- [22] K.P. Goetz, D. Vermeulen, M.E. Payne, C. Kloc, L.E. McNeil, O.D. Jurchescu, Charge-transfer complexes: new perspectives on an old class of compounds, J. Mater. Chem. C 2 (17) (2014) 3065–3076, https://doi.org/10.1039/ C3TC32062F.
- [23] T.J. Kistenmacher, T.E. Phillips, D.O. Cowan, The crystal structure of the 1:1 radical cation–radical anion salt of 2,2'-Bis-I,3-Dithiole (TTF) and 7,7,8,8-tetracyanoquinodimethane (TCNQ), Acta Crystallogr. Sect. B Struct. Crystallogr. Cryst. Chem. 30 (3) (1974) 763–768, https://doi.org/10.1107/S0567740874003669.

- [24] T.J. Emge, F. Mitchell Wiygul, J.P. Ferraris, T.J. Kistenmacher, Crystal structure and madelung energy for the charge-transfer complex tetrathiafulvalene-2,5difluoro-7,7,8,8-tetracyano-p-quinodimethane, TTF-2,5-TCNQF2. Observations on a dimerized segregated stack motif, Mol. Cryst. Liq. Cryst. 78 (1) (1981) 295–310, https://doi.org/10.1080/00268948108082166.
- [25] A.N. Sokolov, T. Friščić, L.R. MacGillivray, Enforced face-to-face stacking of organic semiconductor building blocks within hydrogen-bonded molecular cocrystals, J. Am. Chem. Soc. 128 (9) (2006) 2806–2807, https://doi.org/ 10.1021/ja057939a.
- [26] J. Xu, Z. Yin, L. Zhang, Q. Dong, X. Cai, S. Li, Q. Chen, P. Keoingthong, Z. Li, L. Chen, Z. Chen, W. Tan, Hydrogen-bonding-induced H-aggregation of charge-transfer complexes for ultra-efficient second near-infrared region photothermal conversion, CCS Chem. 4 (7) (2022) 2333–2343, https://doi.org/10.31635/ccschem.021.202101058.
- [27] F. Topić, K. Rissanen, Systematic construction of ternary cocrystals by orthogonal and robust hydrogen and halogen bonds, J. Am. Chem. Soc. 138 (20) (2016) 6610–6616, https://doi.org/10.1021/jacs.6b02854.
- [28] A. Khan, M. Wang, R. Usman, H. Sun, M. Du, C. Xu, Molecular marriage via charge transfer interaction in organic charge transfer Co-crystals toward solid-state fluorescence modulation, Cryst. Growth Des. 17 (3) (2017) 1251–1257, https:// doi.org/10.1021/acs.cgd.6b01636.
- [29] A. Li, J. Wang, Y. Liu, S. Xu, N. Chu, Y. Geng, B. Li, B. Xu, H. Cui, W. Xu, Remarkable pressure-induced emission enhancement based on intermolecular charge transfer in halogen bond-driven dual-component Co-crystals, Phys. Chem. Chem. Phys. 20 (48) (2018) 30297–30303, https://doi.org/10.1039/C8CP06363J.
- [30] D. Vermeulen, L.Y. Zhu, K.P. Goetz, P. Hu, H. Jiang, C.S. Day, O.D. Jurchescu, V. Coropceanu, C. Kloc, L.E. McNeil, Charge transport properties of perylene–TCNQ crystals: the effect of stoichiometry, J. Phys. Chem. C 118 (42) (2014) 24688–24696, https://doi.org/10.1021/jp508520x.
- [31] A. Yusov, A.M. Dillon, M.D. Ward, Hydrogen bonded frameworks: smart materials used smartly, Mol. Syst. Des. Eng. 6 (10) (2021) 756–778, https://doi.org/ 10.1039/D1MF00055A.
- [32] V.A. Russell, M.C. Etter, M.D. Ward, Layered materials by molecular design: structural enforcement by hydrogen bonding in guanidinium alkane- and arenesulfonates, J. Am. Chem. Soc. 116 (5) (1994) 1941–1952, https://doi.org/ 10.1021/ja00084a039.
- [33] Y. Li, S. Tang, A. Yusov, J. Rose, A.N. Borrfors, C.T. Hu, M.D. Ward, Hydrogen-bonded frameworks for molecular structure determination, Nat. Commun. 10 (1) (2019) 4477, https://doi.org/10.1038/s41467-019-12453-6.
- [34] A.M. Pivovar, K.T. Holman, M.D. Ward, Shape-selective separation of molecular isomers with tunable hydrogen-bonded host frameworks, Chem. Mater. 13 (9) (2001) 3018–3031. https://doi.org/10.1021/cm0104452.
- [35] A.C. Soegiarto, M.D. Ward, Directed organization of dye aggregates in hydrogenbonded host frameworks, Cryst. Growth Des. 9 (8) (2009) 3803–3815, https://doi. org/10.1021/cg900578u.
- [36] V.A. Russell, M.C. Etter, M.D. Ward, Guanidinium para-substituted benzenesulfonates: competitive hydrogen bonding in layered structures and the design of nonlinear optical materials, Chem. Mater. 6 (8) (1994) 1206–1217, https://doi.org/10.1021/cm00044a019.
- [37] W. Xiao, C. Hu, M.D. Ward, Isolation and stabilization of a pheromone in crystalline molecular capsules, Cryst. Growth Des. 13 (7) (2013) 3197–3200, https://doi.org/10.1021/cg4005906.
- [38] A.C. Soegiarto, A. Comotti, M.D. Ward, Controlled orientation of polyconjugated guest molecules in tunable host cavities, J. Am. Chem. Soc. 132 (41) (2010) 14603–14616, https://doi.org/10.1021/ja106106d.
- [39] K.T. Holman, A.M. Pivovar, J.A. Swift, M.D. Ward, Metric engineering of soft molecular host frameworks, Acc. Chem. Res. 34 (2) (2001) 107–118, https://doi. org/10.1021/ary202276
- [40] T. Adachi, M.D. Ward, Versatile and resilient hydrogen-bonded host frameworks, Acc. Chem. Res. 49 (12) (2016) 2669–2679, https://doi.org/10.1021/acs. accounts 6b00360
- [41] APEX4, Bruker AXS, Madison, WI, 2020.
- [42] G. Sheldrick, SHELXT integrated space-group and crystal-structure determination, Acta Crystallogr. A 71 (1) (2015) 3–8.
- [43] G.M. Sheldrick, Crystal structure refinement with SHELXL, Acta Crystallogr. C 71 (1) (2015) 3–8, https://doi.org/10.1107/S2053229614024218.
- [44] A.L. Spek, Structure validation in chemical crystallography, Acta Crystallogr. D D65 (2009) 148–155, https://doi.org/10.1107/S090744490804362X.
- [45] P.R. Spackman, M.J. Turner, J.J. McKinnon, S.K. Wolff, D.J. Grimwood, D. Jayatilaka, M.A. Spackman, CrystalExplorer: a program for Hirshfeld surface analysis, visualization and quantitative analysis of molecular crystals, J. Appl. Crystallogr. 54 (3) (2021) 1006–1011, https://doi.org/10.1107/ S1600576721002910.
- [46] M.J. Frisch, G.W. Trucks, H.B. Schlegel, G.E. Scuseria, M.A. Robb, J.R. Cheeseman, G. Scalmani, V. Barone, G.A. Petersson, H. Nakatsuji, X. Li, M. Caricato, A. V. Marenich, J. Bloino, B.G. Janesko, R. Gomperts, B. Mennucci, D.J. Hratch, Gaussian 16, Revision C.01, Gaussian, Inc., Wallingford, CT, 2016.

- [47] R. Dennington, T.A. Keith, J.M. Millam, GaussView, Version 6.0.16, Semichem Inc., Shawnee Mission, KS, 2016.
- [48] B. Shaanan, U. Shmueli, D. Rabinovich, Structure and packing arrangement of molecular compounds. VII. 7,7,8,8-Tetracyanoquinodimethane–Naphthalene (1:1), Acta Crystallogr. Sect. B Struct. Crystallogr. Cryst. Chem. 32 (9) (1976) 2574–2580, https://doi.org/10.1107/S0567740876008297.
- [49] Y. Li, M. Handke, Y.-S. Chen, A.G. Shtukenberg, C.T. Hu, M.D. Ward, Guest exchange through facilitated transport in a seemingly impenetrable hydrogenbonded framework, J. Am. Chem. Soc. 140 (40) (2018) 12915–12921, https://doi. org/10.1021/jacs.8b07065.
- [50] M.J. Horner, K.T. Holman, M.D. Ward, Architectural diversity and elastic networks in hydrogen-bonded host frameworks: from molecular jaws to cylinders, J. Am. Chem. Soc. 129 (47) (2007) 14640–14660, https://doi.org/10.1021/ja0741574.
- [51] V.A. Russell, C.C. Evans, W. Li, M.D. Ward, Nanoporous molecular sandwiches: pillared two-dimensional hydrogen-bonded networks with adjustable porosity, Science 276 (5312) (1997) 575–579, https://doi.org/10.1126/ science.276.5312.575.
- [52] R.E. Long, R.A. Sparks, K.N. Trueblood, The crystal and molecular structure of 7,7,8,8-tetracyanoquinodimethane, Acta Crystallogr. 18 (5) (1965) 932–939, https://doi.org/10.1107/S0365110X65002256.
- [53] Y. Liu, C. Hu, A. Comotti, M.D. Ward, Supramolecular archimedean cages assembled with 72 hydrogen bonds, Science 333 (6041) (2011) 436–440, https://doi.org/10.1126/science.1204369.
- [54] A. Comotti, S. Bracco, P. Sozzani, S.M. Hawxwell, C. Hu, M.D. Ward, Guest molecules confined in amphipathic crystals as revealed by X-ray diffraction and MAS NMR, Cryst. Growth Des. 9 (7) (2009) 2999–3002, https://doi.org/10.1021/ cg900282k.
- [55] Y. Liu, W. Xiao, J.J. Yi, C. Hu, S.-J. Park, M.D. Ward, Regulating the architectures of hydrogen-bonded frameworks through topological enforcement, J. Am. Chem. Soc. 137 (9) (2015) 3386–3392, https://doi.org/10.1021/jacs.5b00534.
- [56] J.B. Torrance, J.E. Vazquez, J.J. Mayerle, V.Y. Lee, Discovery of a neutral-to-ionic phase transition in organic materials, Phys. Rev. Lett. 46 (4) (1981) 253–257, https://doi.org/10.1103/PhysRevLett.46.253.
- [57] F.L. Hirshfeld, Bonded-atom fragments for describing molecular charge densities, Theor. Chim. Acta 44 (2) (1977) 129–138, https://doi.org/10.1007/BF00549096.
- [58] M.A. Spackman, P.G. Byrom, A novel definition of a molecule in a crystal, Chem. Phys. Lett. 267 (3–4) (1997) 215–220, https://doi.org/10.1016/S0009-2614(97) 00100-0.
- [59] J.J. McKinnon, M.A. Spackman, A.S. Mitchell, Novel tools for visualizing and exploring intermolecular interactions in molecular crystals, Acta Crystallogr. Sect. B Struct. Sci. 60 (6) (2004) 627–668, https://doi.org/10.1107/ S0108768104020300.
- [60] R. Usman, A. Khan, H. Sun, M. Wang, Study of charge transfer interaction modes in the mixed donor-acceptor cocrystals of pyrene derivatives and TCNQ: a combined structural, thermal, spectroscopic, and Hirshfeld surfaces analysis, J. Solid State Chem. 266 (2018) 112–120, https://doi.org/10.1016/j.jssc.2018.07.009.
- [61] S. Matsuzaki, R. Kuwata, K. Toyoda, Raman spectra of conducting TCNQ salts; estimation of the degree of charge transfer from vibrational frequencies, Solid State Commun. 33 (4) (1980) 403–405, https://doi.org/10.1016/0038-1098(80)90429-
- [62] T. Takenaka, Molecular vibrational spectra of tetracyanoquinodimethane and tetracyanoquinodimethane-D4 crystals, Spectrochim. Acta Part A Mol. Spectrosc. 27 (9) (1971) 1735–1752, https://doi.org/10.1016/0584-8539(71)80228-3.
- [63] D.L. Jeanmaire, R.P. Van Duyne, Resonance Raman spectroelectrochemistry. 2. Scattering spectroscopy accompanying excitation of the lowest 2B1u excited state of the tetracyanoquinodimethane anion radical, J. Am. Chem. Soc. 98 (14) (1976) 4029–4033, https://doi.org/10.1021/ja00430a001.
- [64] K.P. Goetz, J. Tsutsumi, S. Pookpanratana, J. Chen, N.S. Corbin, R.K. Behera, V. Coropceanu, C.A. Richter, C.A. Hacker, T. Hasegawa, O.D. Jurchescu, Polymorphism in the 1:1 charge-transfer complex DBTTF–TCNQ and its effects on optical and electronic properties, Adv. Electron. Mater. 2 (10) (2016), 1600203, https://doi.org/10.1002/aelm.201600203.
- [65] T.J. Kistenmacher, T.J. Emge, F.M. Wiygul, W.A. Bryden, J.S. Chappell, J.P. Stokes, L.-Y. Chiang, D.O. Cowan, A.N. Bloch, DBTTF-TCNQ: a fractionally-charged organic salt with a mixed-stack crystalline motif, Solid State Commun. 39 (3) (1981) 415–417, https://doi.org/10.1016/0038-1098(81)90630-X.
- [66] J.S. Chappell, A.N. Bloch, W.A. Bryden, M. Maxfield, T.O. Poehler, D.O. Cowan, Degree of charge transfer in organic conductors by infrared absorption spectroscopy, J. Am. Chem. Soc. 103 (9) (1981) 2442–2443, https://doi.org/ 10.1021/ia00399a066.
- [67] J. Tauc, Optical properties and electronic structure of amorphous Ge and Si, Mater. Res. Bull. 3 (1) (1968) 37–46, https://doi.org/10.1016/0025-5408(68)90023-8.
- [68] K. Müller, N. Schmidt, S. Link, R. Riedel, J. Bock, W. Malone, K. Lasri, A. Kara, U. Starke, M. Kivala, M. Stöhr, Triphenylene-derived electron acceptors and donors on Ag(111): formation of intermolecular charge-transfer complexes with common unoccupied molecular states, Small 15 (33) (2019), 1901741, https://doi.org/10.1002/smll.201901741.